Formation of pseudomorphic nanocages from Cu_2O nanocrystals through anion exchange reactions

Hsin-Lun Wu, Ryota Sato, Atsushi Yamaguchi, Masato Kimura, Mitsutaka Haruta, Hiroki Kurata, and Toshiharu Teranishi*
Institute for Chemical Research, Kyoto University, Gokasho, Uji, Kyoto 611-0011, Japan
*Corresponding author. E-mail: teranisi@scl.kyoto-u.ac.jp

The crystal structure of ionic nanocrystals (NCs) is usually controlled by reaction temperature, according to their phase diagram. We show that when ionic NCs with different shapes, but identical crystal structures, were subjected to anion exchange reactions under ambient conditions, pseudomorphic products with different crystal systems were obtained. The shape-dependent anionic framework (surface anion sublattice and stacking pattern) of Cu_2O NCs determined the crystal system of anion-exchanged products of Cu_xS nanocages. This method enabled us to convert a body-centered cubic lattice into either a face-centered cubic or a hexagonally close-packed lattice to form crystallographically unusual multiply-twinned structures. Subsequent cation exchange reactions gave CdS nanocages, while preserving the multiply-twinned structures. High temperature stable phase like wurtzite ZnS was also obtained by this method at ambient conditions.

Chemical conversion of semiconductor NCs via ion exchange reactions can overcome the difficulties associated with controlling the size, shape, chemical composition and crystal structure in conventional syntheses (*1-7*). However, the crystal structure transformation in ion exchange reactions is still not well understood. When the entire crystal is in a structurally non-equilibrium state in ion exchange reactions, both the cations and anions are mobile and can induce morphological changes to the thermodynamically more stable shape prior to reach the final equilibrium state. For ionic NCs above a critical size, the anion framework remains intact and the original shape of the parent-NCs is retained throughout the cation exchange reaction (*8*). The retained shape of the parent-NCs in ion exchange provides an opportunity to obtain non-equilibrium unique structures and even new structures of ionic NCs (*9*), these final structures being known as “pseudomorphs”.

We now show using Cu_2O NCs with well-defined shapes as parent-NCs (*10, 11*), a distinctive shape-dependent anionic frameworks-induced crystal phase transition in anion exchange reaction at ambient conditions. Regular hexahedral (RH) Cu_2O NCs with a cubic phase were converted into RH $Cu_{1.8}S$ nanocages with a cubic phase, while rhombic dodecahedral (RD) Cu_2O NCs with a cubic phase were converted into RD $Cu_{1.75}S$ nanocages with a triclinic phase (*12*) after partial anion exchange reaction. The Cu_2O NCs have a body-centered cubic (bcc) anion sublattice, but they were converted into the Cu_xS nanocages with either a face-centered cubic (fcc) or a hexagonally close-packed (hcp) anion sublattice. Furthermore, shape retention of the Cu_xS pseudomorphic nanocages after the Cu_2O NCs provided new multiply-twinned structures consisting of unusual connections between crystallographically independent walls. Subsequent cation exchange reactions performed on RH and RD Cu_xS nanocages gave RH and RD CdS nanocages with a zincblende and a wurtzite phase, respectively, and preserved the pseudomorphic structures. The wurtzite ZnS nanocages, which formed under ambient conditions, are much more desirable for their optical properties than the zincblende phase (*13, 14*) that are usually synthesized at ~600 °C (*15*).

Scanning electron microscopy (SEM) images, x-ray diffraction (XRD), and ultraviolet-visible-near infrared (UV-Vis-NIR) spectra of the Cu_2O NCs and the Cu_xS and CdS pseudomorphic nanocages

are shown in Fig. 1. All reactions were performed under ambient conditions (*16*). Partial anion exchange reactions of the RH and RD Cu_2O NCs (Fig. 1, A to C) with Na_2S gave cubic RH $Cu_{1.8}S$ and triclinic RD $Cu_{1.75}S$ nanocages (Fig. 1, D and E). The characteristic UV-Vis-NIR spectra of the products (Fig. 1F) confirmed that they were indeed Cu_xS nanocages (*17*). Subsequent cation exchange of RH $Cu_{1.8}S$ nanocages with Cd^{2+} generated the zincblende RH CdS as majority. More accurately, the XRD pattern (Fig. 1E) reflects the large amount of twinning in the RH nanocages and heavily twinned fcc shows up as hcp. On the other hand, the cation exchange of RD $Cu_{1.75}S$ nanocages with Cd^{2+} generated the wurtzite RD CdS nanocages (Fig. 1, G and H). The UV-Vis-NIR spectra displayed the characteristic semiconducting CdS phase (Fig. 1I). Low magnification SEM images of the Cu_xS and CdS nanocages are presented in Fig. S1.

The overall phase transitions starting from the RH and RD Cu_2O NCs are illustrated schematically in Fig. 2. The RH Cu_2O NCs, which were enclosed by six {100} facets (anionic framework: C_4 symmetry, AB stacking), were converted into RH $Cu_{1.8}S$ nanocages with a cubic phase (C_4 symmetry, AB stacking), whereas the RD Cu_2O NCs, which were enclosed by 12 {110} facets (C_2 symmetry, AB stacking), were converted into RD $Cu_{1.75}S$ nanocages with a triclinic phase (C_2 symmetry, ABA′B′ stacking) (*12*). Subsequent cation exchange reactions, in which the Cu^+ was replaced with Cd^{2+}, predominately conserved the anionic frameworks (*5, 6, 19*), that is, the RH $Cu_{1.8}S$ nanocages gave RH CdS nanocages with a cubic zincblende phase (C_4 symmetry, AB stacking) and the $Cu_{1.75}S$ nanocages gave RD CdS nanocages with a hexagonal wurtzite phase (C_2 symmetry, AB stacking).

A detailed examination of the nanocage crystal structures by TEM revealed that the walls consisted of lattice structures with unusual directions and distinctive interwall crystallographic connections. Images of RH $Cu_{1.8}S$ and CdS nanocages are shown in Fig. 3, A and G, respectively, and the corresponding nanobeam diffraction (NBD) patterns from the center of single RH $Cu_{1.8}S$ and CdS nanocages are shown in Fig. 3, B and H, respectively. The high-resolution (HR) TEM image (white square region, Fig. 3A) shown in Fig. 3C revealed lattice fringe spacing of 0.28 and 0.19 nm, corresponding to the (200) and (220) lattice planes of a cubic phase, respectively, indicating that the faces of the walls were the (001) planes. The HR-TEM image of the walls of the $Cu_{1.8}S$ nanocages revealed a cubic phase with a [110] direction to the edge and a [100] direction to the corner (Fig. 3A, yellow arrow). Crystal planes in RH nanostructures with a cubic phase normally displayed a [110] direction parallel to the diagonal line and a [100] direction parallel to the edge line.

Because of the pseudomorphic transformation in anion exchange reaction, the walls in our RH $Cu_{1.8}S$ nanocages are inclined 45° to commonly observed lattice planes (*20*). The crystal structure of the walls of the nanostructures viewed over the faces and the sides are shown in Fig. 4. The anion sublattice viewed over the face of the RH Cu_2O NC (Fig. 4A) has a bcc structure, whereas the anion sublattice of the RH $Cu_{1.8}S$ nanocage (Fig. 4B) has an fcc structure. Both unit cells displayed a similar anionic framework, but the $Cu_{1.8}S$ unit cell was rotated 45° with respect to the Cu_2O unit cell. The rotation observed in the unit cell of the RH $Cu_{1.8}S$ nanocages was caused by the similarity of the surface anion sublattice symmetry and stacking way to those of the RH Cu_2O NCs.

To understand the crystallographic relation between the neighboring walls of the nanocages, we took the fast Fourier transform (FFT) patterns from the face and side of the wall (Fig. 4B). As discussed previously, the face of the RH $Cu_{1.8}S$ nanocage was assigned to the (001) plane and the [100] and [110] directions were parallel to the diagonal and edge lines, respectively. The FFT pattern of the side revealed that the wall was formed by stacking the (100) planes in the [100] direction, and that the wall sides were composed of stacked (110) planes in the [110] direction. Thus, the (001) face of a single wall was parallel to the (011) side of the neighboring wall, meaning that each wall was

crystallographically independent. Thus, single crystal Cu_2O was converted into multiply-twinned $Cu_{1.8}S$ through the anion exchange reaction. The speculated connections between the neighboring walls is depicted schematically in Fig. S2A, in which the (001) and (011) faces are connected through a coherent junction with similarly arranged anions. Subsequent cation exchange reaction, in which Cd^{2+} replaced Cu^{+}, preserved the unusual directions and distinctive interwall crystallographic connections. The HR-TEM image of the RH CdS nanocage revealed lattice fringe spacing of 0.28 and 0.22 nm, corresponding to (200) and (220) lattice planes of zincblende CdS, respectively (Fig. 3I). The FFT patterns of the face and side of the walls of the RH CdS nanocage (Fig. 4C) were similar to those of the RH $Cu_{1.8}S$ nanocage. The unusual rotation of the unit cell was maintained, suggesting that the RH CdS nanocages had a similar interwall connection (Fig. S2A). Moreover, the sides of the walls displayed a similar lattice stacking way (AB) following the ion exchange reactions (Fig. 4, A to C).

Details of the structural transformations that occurred to the RD Cu_2O NCs after the ion exchange were revealed through TEM images; those for RD $Cu_{1.75}S$ and CdS nanocages are shown in Fig. 3, D and J, respectively. The corresponding NBD patterns from the center of single RD $Cu_{1.75}S$ and CdS nanocages are shown in Fig. 3, E and K, respectively. The HR-TEM image (square region, Fig. 3D) shown in Fig. 3F revealed lattice fringe spacing of 0.33 and 0.19 nm, corresponding to the (400) and $(00\bar{8})$ lattice planes of a triclinic phase, respectively (*12*), indicating that the faces of the walls were the (010) planes. The anion sublattice viewed over the face of the RD Cu_2O NC displayed a two-fold symmetry (AB stacking) with a bcc structure (Fig. 4D). The anion sublattice of the (010) face of the RD $Cu_{1.75}S$ nanocage displayed a superimposed pseudo-hexagonal symmetry, more precisely C_2 symmetry (ABA′B′ stacking) with an hcp-like structure (Fig. 4E).

The similarities between the surface anion sublattice symmetries and stacking way indicated that it was possible to transform the crystal structure from a cubic Cu_2O to triclinic $Cu_{1.75}S$ structure via anion exchange reaction with maintaining the shape. The pseudo-hexagonal symmetry of the anion sublattice in $Cu_{1.75}S$ was similar to a hexagonally symmetrical (0001) plane (AB stacking) of a wurtzite structure. Thus, RD CdS nanocages with a wurtzite structure could be formed by further cation exchange reaction of the RD $Cu_{1.75}S$ nanocages even at ambient temperature (Fig. 4F). The HR-TEM image of the RD CdS nanocage (Fig. 3L) displayed lattice fringe spacing of 0.36 and 0.21 nm, corresponding to $(10\bar{1}0)$ and $(11\bar{2}0)$ lattice planes of a wurtzite CdS nanocage, respectively. The crystallographic relation between the neighboring walls of the RD nanocages was determined from the FFT patterns of the faces and sides of the walls (Fig. 4, E and F). Similar to the RH nanocages, the RD nanocages were also composed of crystallographically independent, or polycrystalline, walls, induced by the pseudomorphic transformation in anion exchange reaction. The connection between neighbouring walls is depicted schematically in Fig. S2B. The lattice stacking way (AB) of the walls was also unchanged following the ion exchange reactions (Fig. 4, D to F). Although the anion sublattices of the $Cu_{1.75}S$ nanocage in layer A′ and B′ are slightly distorted (Fig. S3), the symmetry of the anion sublattices still closely resembles the layers A and B. In addition, the volumes of the ion exchanged products expanded, because of the larger radii of S^{2-} and Cd^{2+} (Table S1) (*21*).

One of the advantages of this phase transition method is to selectively obtain polymorphic crystal phases at ambient conditions. The phase transition from zincblende to wurtzite structure of ZnS takes place at 1020 °C. By this phase transition method, ZnS with a zincblende and a wurtzite phase could be both obtained even at room temperature. Here we conducted the pseudomorphic transformation of the RH and RD Cu_2O to Cu_xS and further to ZnS under ambient conditions. Figure S4A shows the SEM and TEM images of the resulting ZnS nanocages. Similar to the case of the CdS nanocages,

subsequent cation exchange reactions of RH $Cu_{1.8}S$ and RD $Cu_{1.75}S$ nanocages with Zn^{2+} are likely to give the zincblende RH ZnS and the wurtzite RD ZnS nanocages, respectively (Fig. S4B). The UV-Vis-NIR spectra displayed the characteristic semiconducting ZnS phase (Fig. S4C), but showed weakly localized surface plasmon resonance peaks in both ZnS nanocages, indicating that small amounts of the Cu_xS phases were present (*22*). The complete cation exchange did not proceed, but we could demonstrate the potential of our method to produce the unobtainable crystal phases under ambient conditions.

Finally, we emphasize that the validity of our observation is strongly supported by the previous report (*4*) demonstrating an anion exchange of the hexagonal pyramid-shaped ZnO NCs with a wurtzite phase to the ZnS hollow NCs with a wurtzite phase. We envisage that this pseudomorphic transformation method could be applicable to a number of other ionic NCs at ambient temperatures, even if they are high-temperature stable phases like wurtzite ZnS.

Fig. 1. Characterization and optical properties of the nanostructures. (A) SEM images, **(B)** XRD patterns, and **(C)** UV-Vis-NIR spectra of the RH and RD Cu_2O NCs. The UV-Vis-NIR spectra shows the characteristic extinction feature of Cu_2O NCs, in which a band gap absorption band was observed at around 450 nm (*10*). **(D)** SEM images, **(E)** XRD patterns, and **(F)** UV-Vis-NIR spectra of the Cu_xS pseudomorphic nanocages obtained by partially sulfiding Cu_2O NCs with Na_2S solution to form Cu_2O-Cu_xS core-shell (Cu_2O@Cu_xS) NCs, followed by etching the interior Cu_2O cores with HCl solution. **(G)** SEM images, **(H)** XRD patterns, and **(I)** UV-Vis-NIR spectra of the CdS pseudomorphic nanocages obtained by further cation exchange of the Cu_xS nanocages with Cd^{2+} (*8*). The UV-Vis-NIR spectra show the clear band gap absorption bands characteristic of CdS nanocages at approximately 460 nm (*18*).

Fig. 2. Schematic illustration for phase transitions induced by the shape-dependent anionic frameworks in anion exchange reactions and the subsequent cation exchange reactions. The crystal structures are projections of the crystal lattice on the faces. Information in parentheses below each structure stands for the symmetry and the stacking way of surface anion sublattices.

Fig. 3. Crystal structure analyses of the walls of nanocages. (A, G) TEM images and **(B, H)** the corresponding NBD patterns viewed over the {200} facets of a single RH $Cu_{1.8}S$ and CdS nanocages, respectively. The NBD spot patterns indicate that the walls of the nanocages are single-crystalline. **(C, I)** HR-TEM images of the square regions of the RH $Cu_{1.8}S$ nanocage in Fig. 3A and the RH CdS nanocage in Fig. 3G. **(D, J)** TEM images and **(E, K)** the corresponding NBD patterns viewed over the {040} and {0002} facets of a single RD $Cu_{1.75}S$ and CdS nanocages, respectively. The NBD spot patterns also indicate that the walls of the nanocages are single-crystalline, as observed in RH nanocages. **(F, L)** HR-TEM images of the square regions of the RD $Cu_{1.8}S$ nanocage in Fig. 3D and the RD CdS nanocage in Fig. 3J.

Fig. 4. Comparison of surface anion sublattice symmetry and stacking way of nanostructures. (A–C) The anion sublattices viewed over the faces of **(A)** the RH Cu_2O NC (bcc structure) with a [100] direction to the edge and a [110] direction to the corner of the wall, **(B)** the RH $Cu_{1.8}S$ nanocage (fcc structure) with a [110] direction to the edge and a [100] direction to the corner of the wall and **(C)** the RH CdS nanocage (fcc structure) with a [110] direction to the edge and a [100] direction to the corner of the wall. The sides of the walls showed the similar lattice stacking way (AB) after a sequence of the ion exchange reactions. **(D–F)** The anion sublattices viewed over the faces of **(D)** the RD Cu_2O NC (bcc structure) with [011] direction to a (011) plane, **(E)** the RD $Cu_{1.75}S$ nanocage (hcp-like structure) with [100] direction to a (010) plane and **(F)** the RD CdS nanocage

(hcp structure) with [01$\bar{1}$0] direction to a (0001) plane. The lattice stacking way (AB) of the walls is also unchanged after a sequence of the ion exchange reactions.

References and Notes:

1. G. D. Moon *et al.,* Chemical transformations of nanostructured materials. *Nano Today* **6,** 186–203 (2011).
2. M. Saruyama *et al.,* Spontaneous formation of wurzite-CdS/zinc blende-CdTe heterodimers through a partial anion exchange reaction. *J. Am. Chem. Soc.*, **133**, 17598–17601 (2011).
3. T. Teranishi, M. Sakamoto, Charge separation in type-II semiconductor heterodimers. *J. Phys. Chem. Lett.*, **4**, 2867–2873 (2013).
4. J. Park, H. Zheng, Y. W. Jun, A. P. Alivisatos, Hetero-epitaxial anion exchange yields single-crystalline hollow nanoparticles. *J. Am. Chem. Soc.* **131,** 13943–13945 (2009).
5. P. K. Jain, L. Amirav, S. Aloni, A. P. Alivisatos, Nanoheterostructure cation exchange: Anionic framework conservation. *J. Am. Chem. Soc.* **132,** 9997–9999 (2010).
6. H. B. Li *et al.,* Sequential cation exchange in nanocrystals: Preservation of crystal phase and formation of metastable phases. *Nano Lett.* **11,** 4964–4970 (2011).
7. D. D. Zhang *et al.,* Phase-selective cation-exchange chemistry in sulfide nanowire systems. *J. Am. Chem. Soc.* **136,** 17430–17433 (2014).
8. D. H. Son, S. M. Hughes, Y. D. Yin, A. P. Alivisatos, Cation exchange reactions in ionic nanocrystals. *Science* **306,** 1009–1012 (2004).
9. R. D. Robinson *et al.,* Spontaneous superlattice formation in nanorods through partial cation exchange. *Science* **317,** 355–358 (2007).
10. W. C. Huang, L. M. Lyu, Y. C. Yang, M. H. Huang, Synthesis of Cu_2O nanocrystals from cubic to rhombic dodecahedral structures and their comparative photocatalytic activity. *J. Am. Chem. Soc.* **134,** 1261–1267 (2012).
11. C. H. Kuo, M. H. Huang, Facile synthesis of Cu_2O nanocrystals with systematic shape evolution from cubic to octahedral structures. *J. Phys. Chem. C* **112,** 18355–18360 (2008).
12. W. G. Mumme, R. W. Gable, V. Petricek, The crystal structure of roxbyite, $Cu_{58}S_{32}$. *Can. Mineral.* **50,** 423–430 (2012).
13. S. B. Qadri *et al.,* The effect of particle size on the structural transitions in zinc sulfide. *J. Appl. Phys.* **89,** 115–119 (2001).
14. Z. W. Wang *et al.*, Morphology-tuned wurtzite-type ZnS nanobelts. *Nat. Mater.* **4,** 922–927 (2005).
15. S. B. Qadri *et al.,* Size-induced transition-temperature reduction in nanoparticles of ZnS. *Phys. Rev. B* **60,** 9191–9193 (1999).
16. Materials and methods are available as Supplementary Materials on *Science* Online.
17. C. H. Kuo, Y. T. Chu, Y. F. Song, M. H. Huang, Cu_2O nanocrystal-templated growth of Cu_2S nanocages with encapsulated Au nanoparticles and in-situ transmission X-ray microscopy study. *Adv. Funct. Mater.* **21,** 792–797 (2011).
18. W. W. Yu, X. G. Peng, Formation of high-quality CdS and other II-VI semiconductor nanocrystals in noncoordinating solvents: Tunable reactivity of monomers. *Angew. Chem. Int. Edit.* **41,** 2368–2371 (2002).
19. M. Kanehara, H. Arakawa, T. Honda, M. Saruyama, T. Teranishi, Large-scale synthesis of high-quality metal sulfide semiconductor quantum dots with tunable surface-plasmon resonance frequencies. *Chem. Eur. J.* **18**, 9230–9238 (2012).
20. C. H. Kuo, C. H. Chen, M. H. Huang, Seed-mediated synthesis of monodispersed Cu_2O nanocubes with five different size ranges from 40 to 420 nm. *Adv. Funct. Mater.* **17,** 3773–3780

(2007).
21. J. B. Rivest, P. K. Jain, Cation exchange on the nanoscale: an emerging technique for new material synthesis, device fabrication, and chemical sensing. *Chem. Soc. Rev.* **42**, 89–96 (2013).
22. D. H. Ha *et al.,* Solid-solid phase transformations induced through cation exchange and strain in 2D heterostructured copper sulfide nanocrystals. *Nano Lett.* **14**, 7090–7099 (2014).

Acknowledgements
This work was partly supported by the Artificial Photosynthesis Project (ARPChem) of the New Energy and Industrial Technology Development Organization (NEDO) of Japan.

Supplementary Materials:

Materials and Methods

Fig. S1-S4

Tables S1

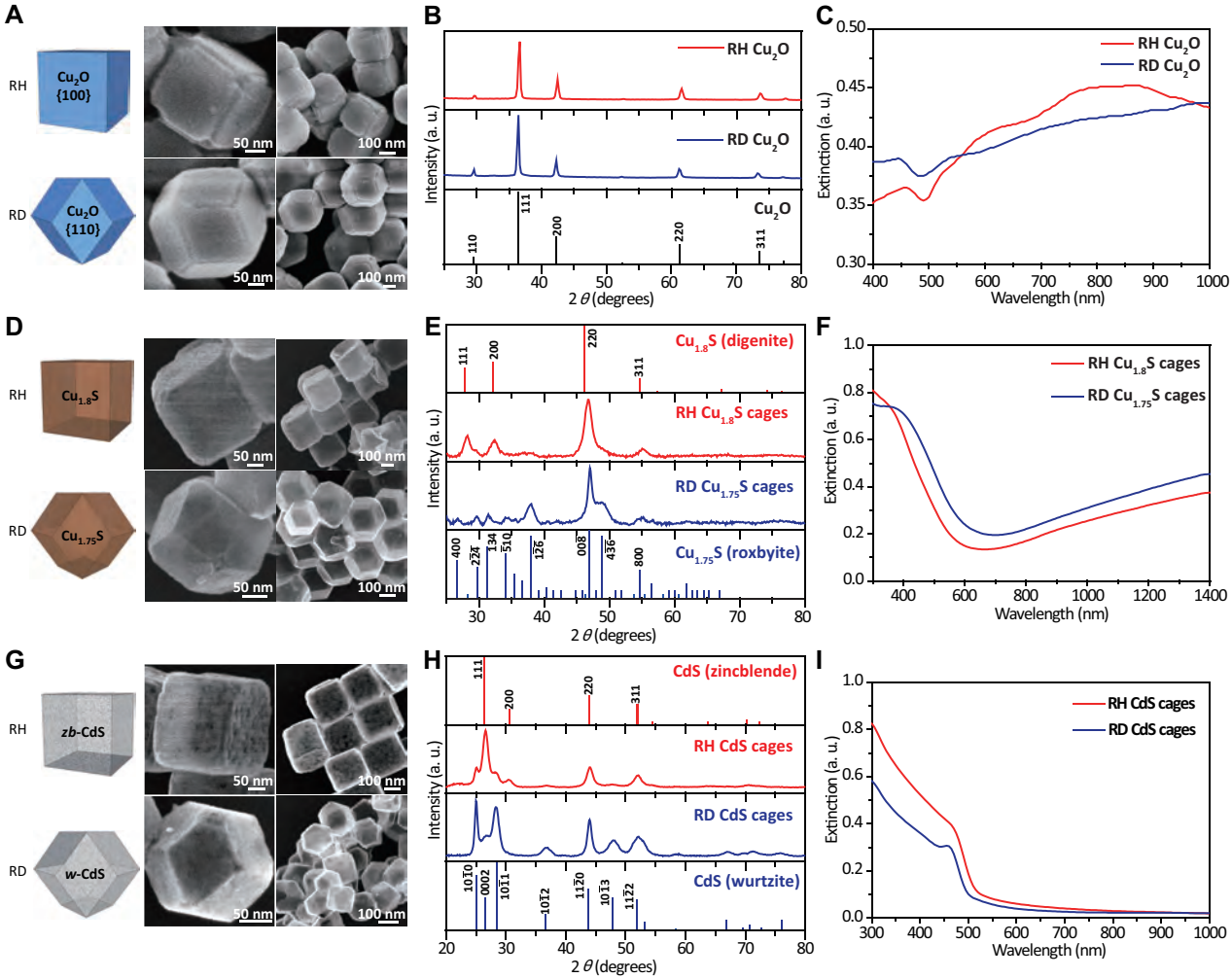
A
RH
Cu2O {100}
RD
Cu2O {110}
50 nm
100 nm
B
RH Cu2O
RD Cu2O
Cu2O
Intensity (a. u.)
110
111
200
220
311
2θ (degrees)
C
RH Cu2O
RD Cu2O
Extinction (a. u.)
Wavelength (nm)
D
RH
Cu1.8S
RD
Cu1.75S
E
Cu1.8S (digenite)
RH Cu1.8S cages
RD Cu1.75S cages
Cu1.75S (roxbyite)
F
RH Cu1.8S cages
RD Cu1.75S cages
G
RH
zb-CdS
RD
w-CdS
H
CdS (zincblende)
RH CdS cages
RD CdS cages
CdS (wurtzite)
I
RH CdS cages
RD CdS cages

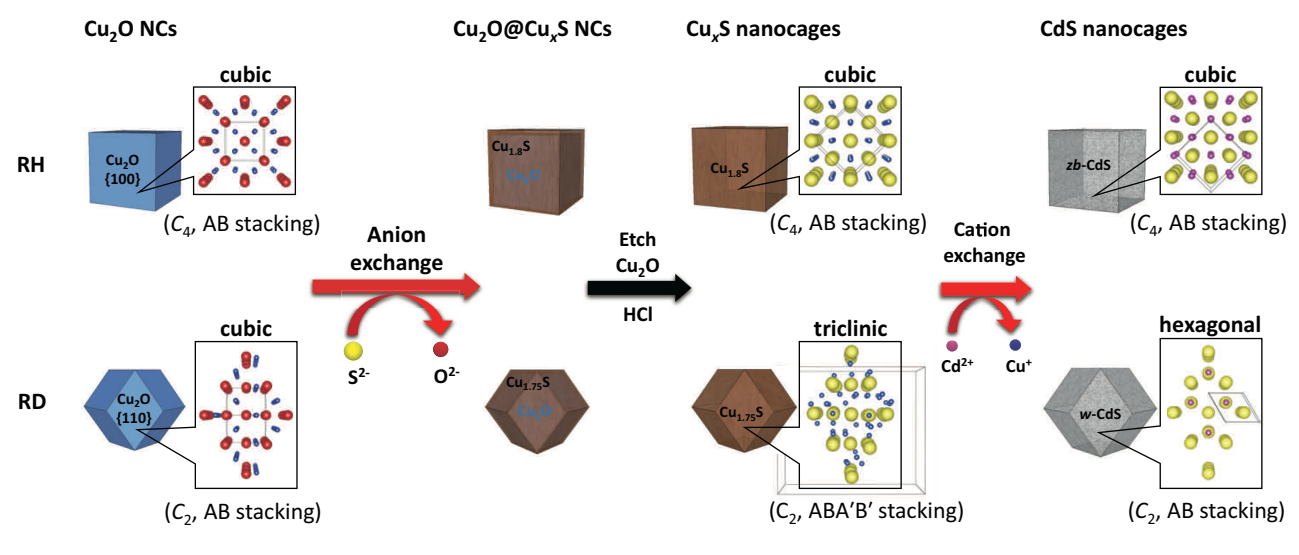
Cu2O NCs
Cu2O@CuxS NCs
CuxS nanocages
CdS nanocages
RH
RD
cubic
Cu2O {100}
(C4, AB stacking)
Anion exchange
S2-
O2-
Cu1.8S
Cu2O
Etch Cu2O
HCl
Cu1.8S
(C4, AB stacking)
Cation exchange
Cd2+
Cu+
zb-CdS
(C4, AB stacking)
cubic
Cu2O {110}
(C2, AB stacking)
Cu1.75S
Cu2O
triclinic
Cu1.75S
(C2, ABA'B' stacking)
hexagonal
w-CdS
(C2, AB stacking)

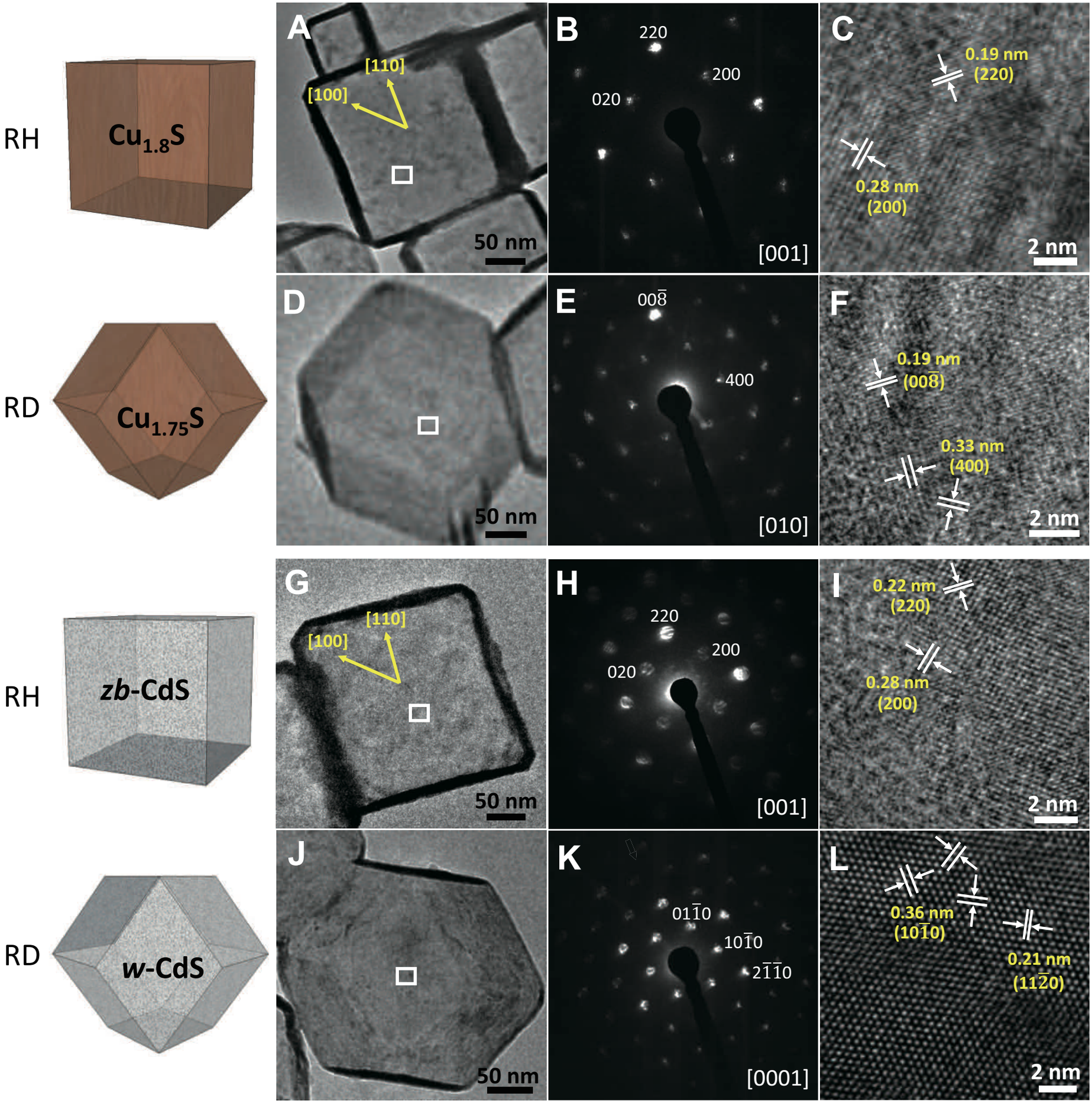
RH
Cu1.8S
RD
Cu1.75S
RH
zb-CdS
RD
w-CdS
A
[110]
[100]
50 nm
B
220
200
020
[001]
C
0.19 nm
(220)
0.28 nm
(200)
2 nm
D
50 nm
E
00$\bar{8}$
400
[010]
F
0.19 nm
(00$\bar{8}$)
0.33 nm
(400)
2 nm
G
[110]
[100]
50 nm
H
220
200
020
[001]
I
0.22 nm
(220)
0.28 nm
(200)
2 nm
J
50 nm
K
01$\bar{1}$0
10$\bar{1}$0
2$\bar{1}\bar{1}$0
[0001]
L
0.36 nm
(10$\bar{1}$0)
0.21 nm
(11$\bar{2}$0)
2 nm

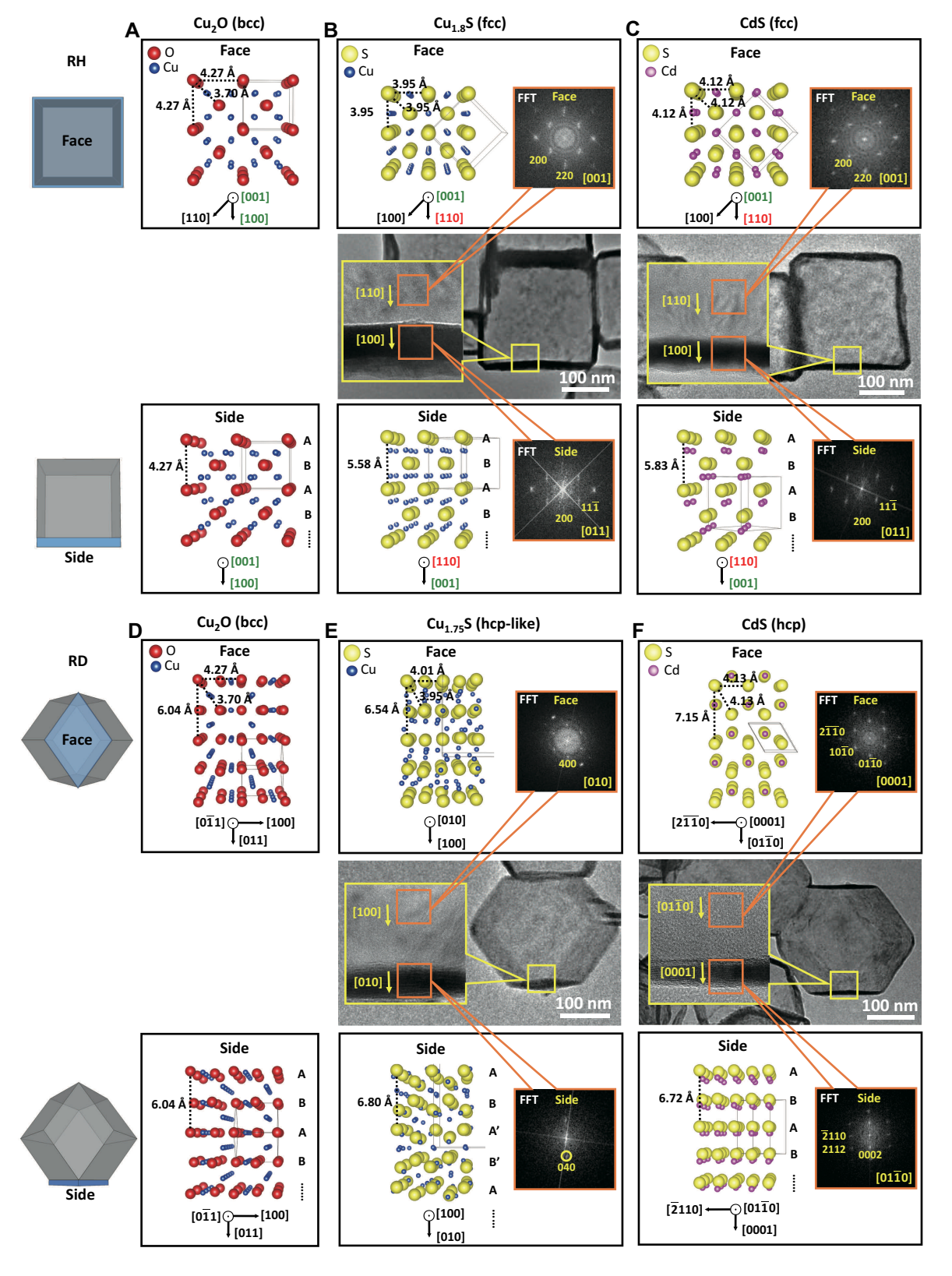
A
Cu2O (bcc)
B
Cu1.8S (fcc)
C
CdS (fcc)
RH
Face
O
Cu
S
Cd
4.27 Å
3.70 Å
3.95 Å
4.12 Å
FFT
200
220
[001]
[110]
[100]
100 nm
Side
5.58 Å
5.83 Å
A
B
111
011
D
Cu2O (bcc)
E
Cu1.75S (hcp-like)
F
CdS (hcp)
RD
4.01 Å
6.54 Å
400
010
4.13 Å
7.15 Å
2110
1010
0110
0001
6.04 Å
6.80 Å
6.72 Å
A'
B'
040
0002

Supplementary Materials for

Formation of pseudomorphic nanocages from Cu_2O nanocrystals through anion exchange reactions

Hsin-Lun Wu, Ryota Sato, Atsushi Yamaguchi, Masato Kimura, Mitsutaka Haruta, Hiroki Kurata, and Toshiharu Teranishi*

correspondence to: teranisi@scl.kyoto-u.ac.jp

This PDF file includes:

Materials and Methods

Chemicals

Copper(II) nitrate trihydrate ($Cu(NO_3)_2 \square 3H_2O$, 99%, Wako), hydroxylammonium chloride ($NH_2OH \square HCl$, 98%, Wako), sodium hydroxide (NaOH, 96%, Wako), sodium dodecyl sulfate (SDS, 99+%, Aldrich), sodium sulfate, 9-hydrate ($Na_2S \square 9H_2O$, 98%, Chamekon Reagent), hydrochloric acid (HCl, 35~37%, nacalai tesque), cadmium nitrate tetrahydrate ($Cd(NO_3)_2 \square 4H_2O$, 99.9%, Wako), tributyl phosphine (TBP, 99+%, TCI), Trioctylphosphine (TOP, 95%, Kanto Chemical), methanol (99.9%, Wako), toluene (99.8%, Wako) and n-octylamine (99.5%, Wako) were used without further purification. Ultrapure distilled and deionized water was used for all solution preparations.

Methods

Synthesis of RH and RD Cu_2O NCs. $Cu(NO_3)_2$ (0.1 M, 50 μmol), SDS surfactant (0.03 M, 0.3 mmol), $NH_2OH \cdot HCl$ aqueous solution (0.2 M, 40 μmol for RH and 240 μmol for RD) and NaOH (1.0 M, 180 μmol) were added to a vial in the order listed and the mixture was held for 2 h at 23 °C. The reaction mixture was purified by centrifugation at 5000 rpm for 10 min. The precipitate was washed using methanol (5 mL), then subjected to centrifugation at 5000 rpm for 5 min. The final product was redispersed in methanol (5 mL).

Synthesis of RH and RD Cu_xS Nanocages. The as-synthesized Cu_2O NCs in methanol (5 mL) were cooled in an ice-bath for 5 min. $Na_2S_{(aq)}$ (100 μL, 0.05 M, 5.0 μmol) was added to the suspension, then stirred for 30 s to convert the surfaces of the Cu_2O NCs into thin Cu_xS shells (~ 8 nm). The suspension was centrifuged at 5000 rpm for 5 min, then the precipitate was dispersed in methanol (5 mL). The Cu_2O cores were removed by adding $HCl_{(aq)}$ (100 μL, 2.0 M, 200 μmol) with shaking for 30 s. The solution turned brown immediately, indicating the formation of Cu_xS nanocages. The nanocage suspension was centrifuged at 5000 rpm for 10 min, then redispersed in methanol (5 mL) for the subsequent cation exchange reaction from Cu_xS to CdS.

Synthesis of RH and RD CdS Nanocages. A mixture of $Cd(NO_3)_2$ in methanol (2.5 mL, 0.2 M, 0.5 mmol) and TBP in toluene (2.5 mL, 0.4 M, 1.0 mmol) was added dropwise to the Cu_xS nanocage solution at ambient temperature under sonication. The exchange reaction was allowed to proceed for 30 min, with the brown solution gradually turning yellow. The CdS nanocage suspension was centrifuged at 6500 rpm for 10 min twice, then redispersed in methanol (5 mL).

Synthesis of RH and RD ZnS Nanocages. A mixture of $Zn(NO_3)_2$ in methanol (2.5 mL, 0.2 M, 0.5 mmol) and TOP in toluene (2.5 mL, 0.4 M, 1.0 mmol) was added dropwise to the Cu_xS nanocage solution at ambient temperature under sonication. The exchange reaction was allowed to proceed for 2 h. The ZnS nanocage suspension was centrifuged at 6500 rpm for 10 min twice, then redispersed in methanol (5 mL).

Characterization

Scanning electron microscopy (SEM) images of the samples were obtained using a S-4800 (HITACHI) electron microscope. Transmission electron microscopy (TEM) characterization was performed on JEM1011 (JEOL) and JEOL-2200 (FS equipped with Cs-corrector) electron microscopes with operating voltages of 100 kV and 200 kV. Powder X-ray diffraction (XRD) patterns were recorded on a PANalytical X'Pert Pro MPD diffractometer with Cu Kα radiation. UV-vis absorption spectra were taken using a U-4100 (HITACHI) spectrophotometer.

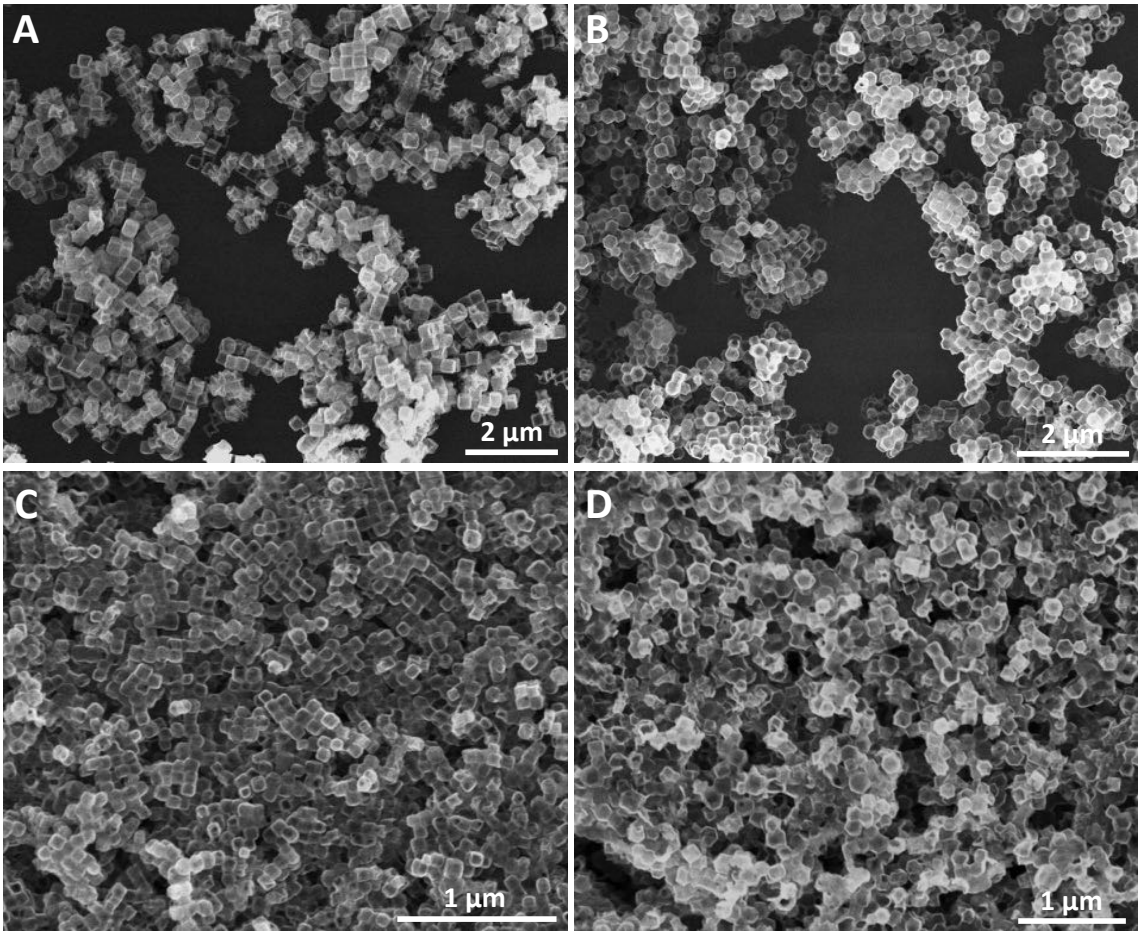

Fig. S1 Low magnification SEM images of (A) RH $Cu_{1.8}S$, (B) RD $Cu_{1.75}S$, (C) RH CdS, and (D) RD CdS nanocages.

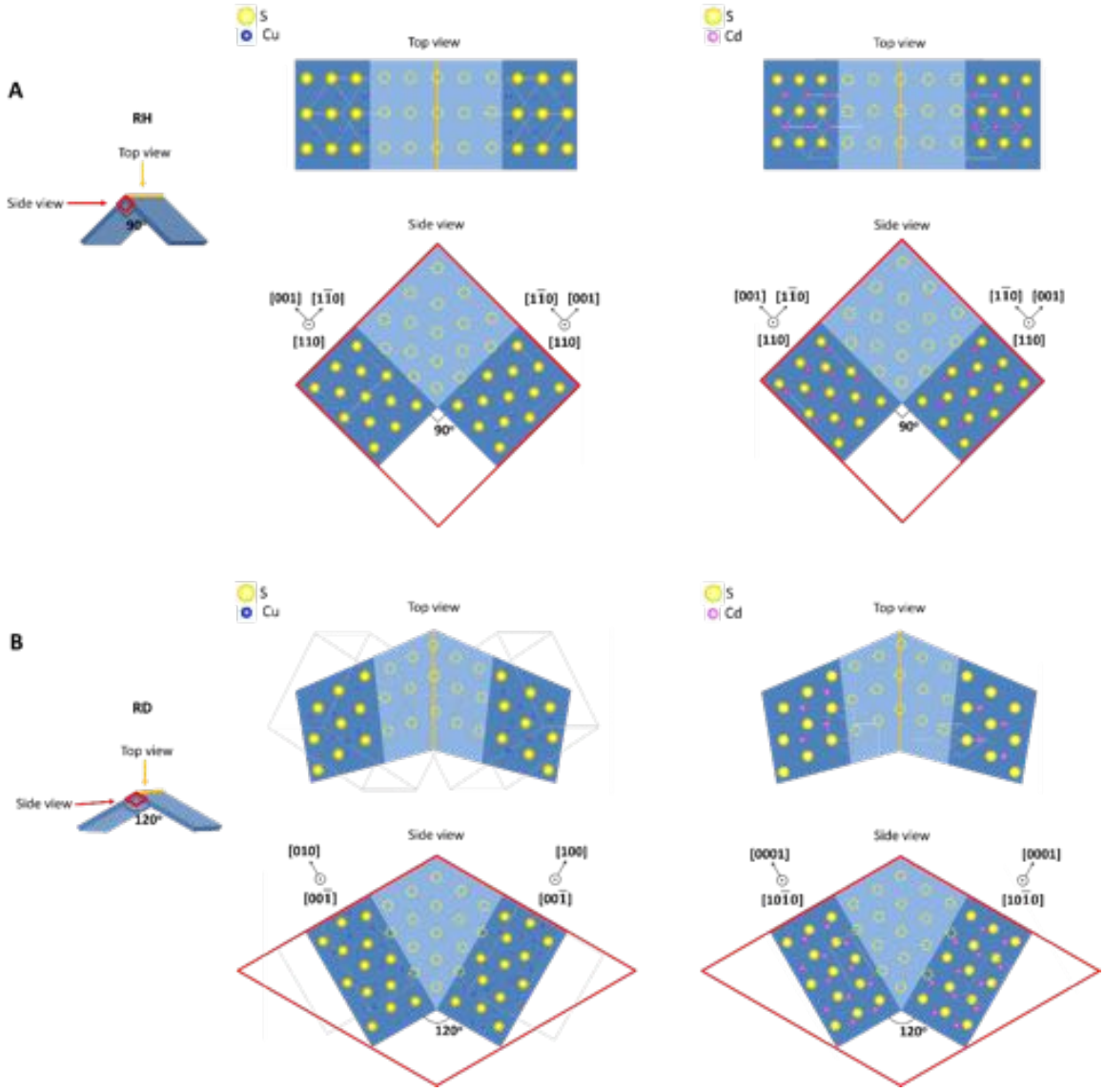

Fig. S2 The connections of two neighboring walls viewed from the orange lines (top view) and the red squares (side view) in (A) RH and (B) RD nanocages. The yellow dotted circles stand for the speculated anion arrangements in the connected areas.

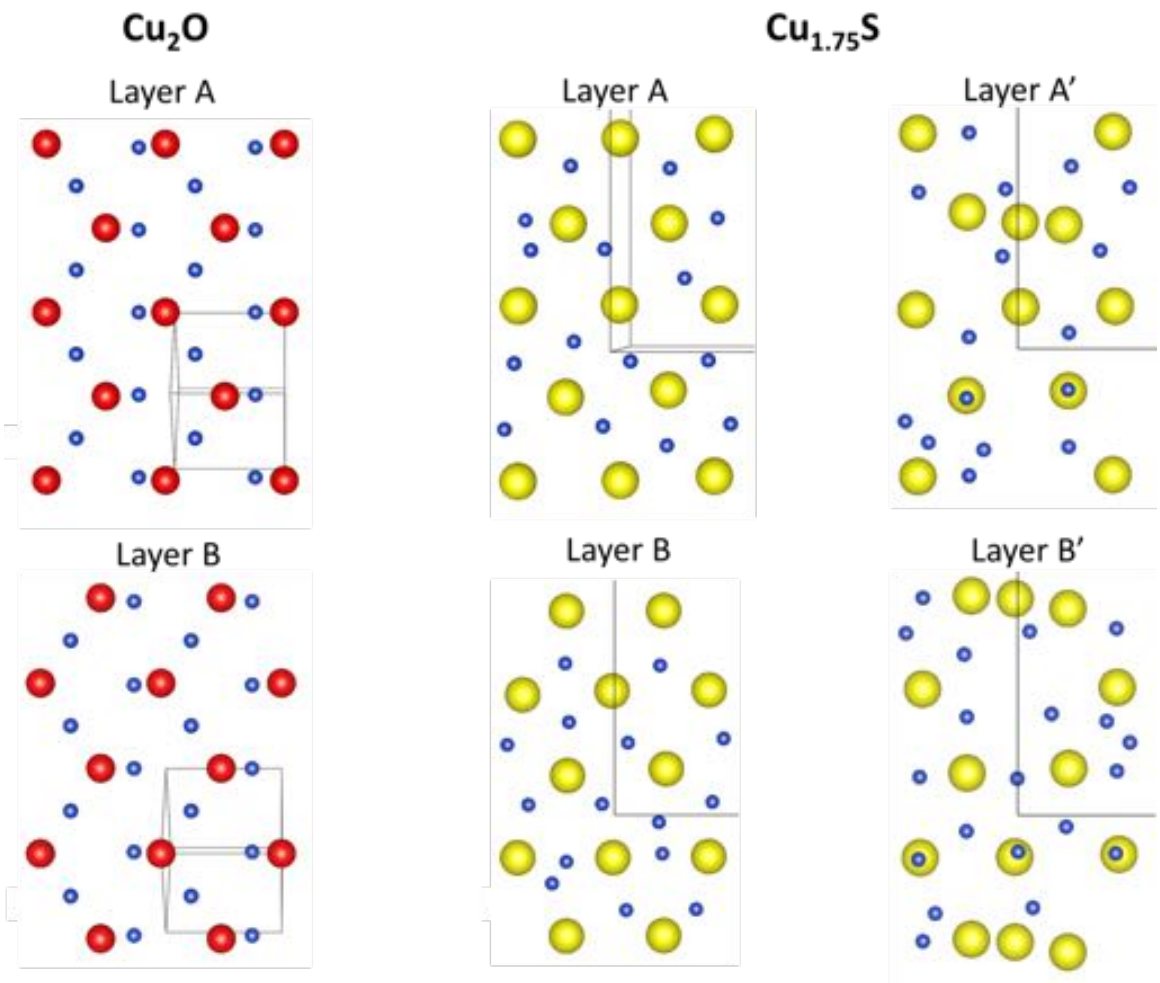

Fig. S3 The stacking faces of the RD Cu_2O NC and $Cu_{1.75}S$ nanocage shown in Fig. 4, D and E.

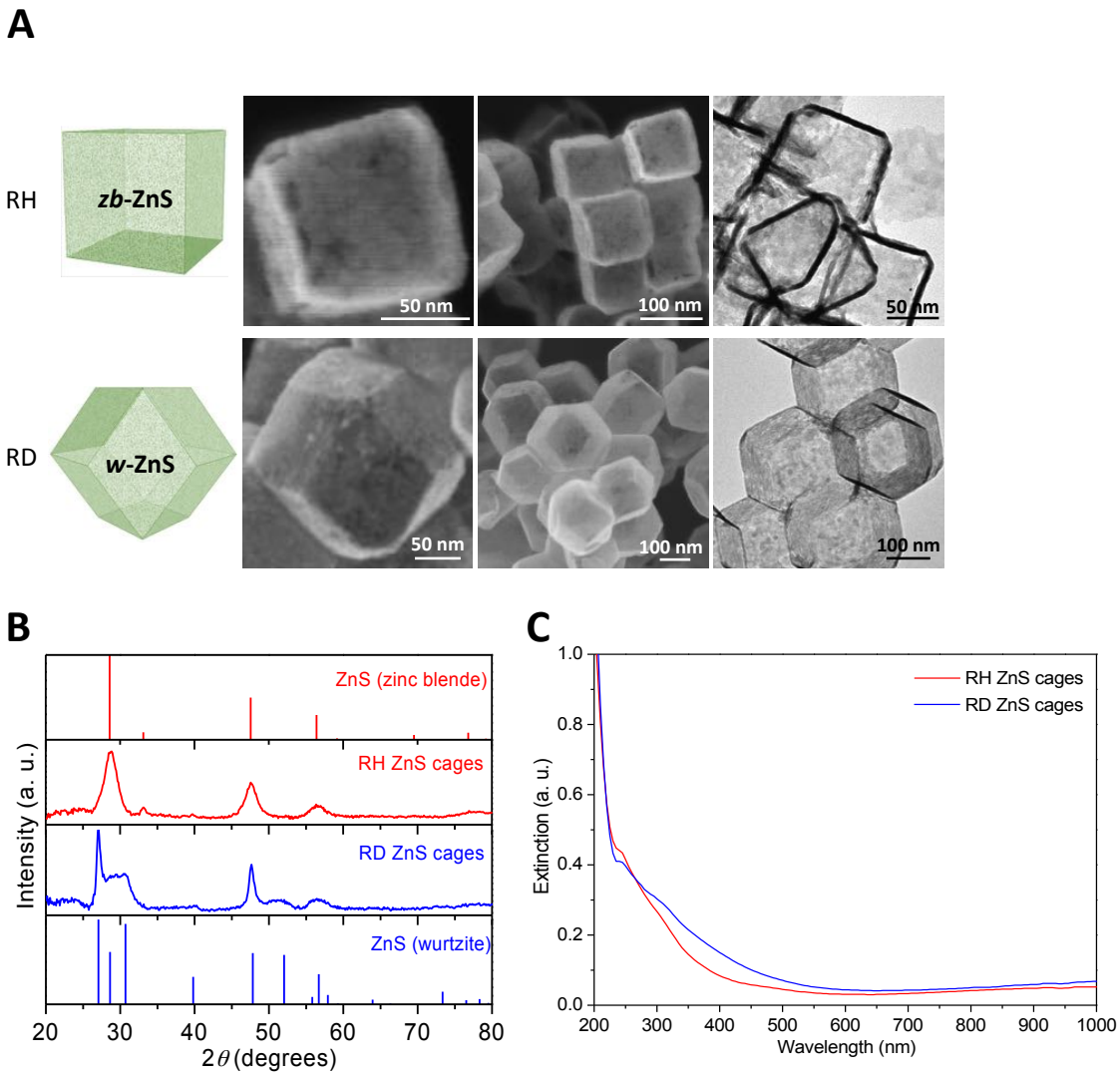

Fig. S4 ZnS nanocages with different crystal structures obtained from the shape-dependent anionic frameworks induced phase transitions. (A) SEM and TEM images, (B) XRD patterns, and (C) UV-Vis-NIR spectra of the ZnS nanocages obtained by cation exchange of the Cu_xS nanocages with Zn^{2+}.

	RH	RD
Cu_2O	0.026 (anion· $Å^{-3}$)	0.026 (anion· $Å^{-3}$)
Cu_xS	0.023 (anion· $Å^{-3}$)	0.023 (anion· $Å^{-3}$)
CdS	0.020 (anion· $Å^{-3}$)	0.020 (anion· $Å^{-3}$)

Table S1 Comparison of anion densities of the RH and RD nanostructures after ion exchange reactions.